Table 4. *Permutation table of the beams of example* 3 (*see Fig.* 8)

$p4m$	1	4^1	2	4^3	m_x	m_y	m_{xy}	$m_{x\bar{y}}$
	χ	q_1	q_2	q_3	q_3	q_1	χ	q_2
	q_1	q_2	q_3	χ	q_2	χ	q_3	q_1
	q_2	q_3	χ	q_1	q_1	q_3	q_2	χ
	q_3	χ	q_1	q_2	χ	q_2	q_1	q_3
Γ	4	0	0	0	0	0	2	2

VI. Concluding remarks

The quantum-mechanical formalism of the dynamical theory of fast-electron elastic scattering provides an elegant tool for understanding the main features of the symmetry properties of the Hamiltonian.

The basic idea of the present description is to express all symmetry operators directly in Hilbert space in order to use essentially intuitive geometric pictures for finding the symmetry-adapted basis.

As expected, the elastic Hamiltonian being real, one can always find a basis on which the scattering matrix is real. Each time a reflection is in a Bragg position, the real basis has the same size as the natural $\{|\mathbf{q}\rangle\}$ basis. The 2_1-fold dynamical extinction is an illustration of the non-trivial case $\mathcal{R}^2 = -1$ anti-unitary operation in Wigner's original work.

Applied to unitary transformations, the present technique leads to the same kind of beam reduction as developed by Takeda (1986, 1987) and is especially powerful for high-symmetry orientations. The systematic construction of the Hamiltonian matrix elements can be performed by a simple diagrammatic scheme where the self excitation (diagonal element) is replaced by a summation (with appropriate signs for non-symmorphic space groups) over all the internal coupling potentials of the beams of the orbit, and the off-diagonal elements between two different orbits are obtained by a summation of the coupling potentials between one chosen beam of the first orbit and all the beams of the second orbit.

References

BERRY, M. V. (1971). *J. Phys. C*, **4**, 697-722.

BLUME, J. (1966). *Z. Phys.* **191**, 248-253.

BUXTON, B. F., EADES, J. A., STEEDS, J. W. & RACKHAM, G. M. (1976). *Philos. Trans. R. Soc. London*, **281**, 171-194.

CORNIER, M., PORTIER, R. & GRATIAS, D. (1986). Proc. XIth Int. Congr. on Electron Microscopy, Kyoto, pp. 195-198.

COWLEY, J. M. (1975). *Diffraction Physics*. New York: North-Holland.

COWLEY, J. M. & MOODIE, A. F. (1957). *Acta Cryst.* **10**, 609-619.

EADES, J. A. (1980). *Physics of Modern Materials*, Vol. 1. Vienna: IAEA.

FISHER, P. M. (1968). *Jpn. J. Appl. Phys.* **7**, 191-199.

FUKUHARA, A. (1966). *J. Phys. Soc. Jpn*, **21**, 2645-2662.

GJØNNES, J. & MOODIE, A. F. (1965). *Acta Cryst.* **19**, 65.

GOODMAN, P. & MOODIE, A. F. (1974). *Acta Cryst.* **A30**, 280-290.

GRATIAS, D. & PORTIER, R. (1983). *Acta Cryst.* **A39**, 576-584.

HOWIE, A. & WHELAN, M. J. (1961). *Proc. R. Soc. London Ser. A*, **263**, 217-237.

KAMBE, K. (1967). *Z. Naturforsch. Teil A*, **22**, 422-431.

KOGISO, M. & TAKAHASHI, H. (1977). *J. Phys. Soc. Jpn.* **42**, 223-229.

MESSIAH, A. (1965). *Mécanique Quantique*. Paris: Dunod.

SEITZ, F. (1936). *Ann. Math. Stat.* **37**, 17-35.

STURKEY, L. (1957). *Acta Cryst.* **10**, 858-859.

STURKEY, L. (1962). *Proc. Phys. Soc. London*, **80**, 321-354.

TAKEDA, M. (1986). Proc. XIth Int. Congr. on Electron Microscopy, Kyoto, pp. 749-751.

TAKEDA, M. (1987). *Phys. Status Solidi A*, **101**, 25-36.

TINNAPPEL, A. & KAMBE, K. (1975). *Acta Cryst.* **A31**, S6.

TOURNARIE, M. (1960). *Bull. Soc. Fr. Minéral. Cristallogr.* **83**, 179-186.

VAN DYCK, D. (1980). *J. Microsc.* **119**, 141-152.

VERGASOV, V. L., CHUKHOBSKII, F. N. & PINSKER, Z. G. (1982). *Kristallografiya*, **27**, 446-456.

WIGNER, E. P. (1932). *Göttinger Nachr.* **31**, 546-559.

Acta Cryst. (1988). **A44**, 798-805

Imaging Tunnel Atoms in Intergrowth Tungsten Bronzes

BY LARS KIHLBORG AND MARGARETA SUNDBERG

Department of Inorganic Chemistry, Arrhenius Laboratory, University of Stockholm, S-10691 Stockholm, Sweden

(*Received* 5 *January* 1988; *accepted* 6 *April* 1988)

Abstract

Crystals of caesium and rubidium intergrowth tungsten bronze (ITB) have been studied by high-resolution electron microscopy. The structure of these consists of slabs of WO_3 type, intergrown with slabs of hexagonal tungsten bronze (HTB) type containing hexagonal tunnels in which the alkali atoms are accommodated. In the images of thicker parts the hexagonal tunnels are clearly revealed. In the thin parts the HTB structure mostly appears as a hexagonal pattern of dots of equal intensity and the tunnels are not recognizable. This applies particularly to Cs ITB but also in many instances to Rb ITB. Image simulations, assuming known or estimated degrees of filling of the tunnels with alkali, show a clear difference in contrast at the tungsten and alkali positions, especially at certain focus settings. The dis-

0108-7673/88/060798-08$03.00

crepancy is thought to be due to surface reconstruction, whereby tungsten atoms are trapped in the tunnels or the surface layers are shifted, making the surface structure similar to that of $WO_3.\frac{1}{3}H_2O$.

Introduction

High-resolution electron microscopy (HREM) has established itself as an invaluable tool for determination of the local structure of thin crystalline species. The interpretation of HREM images can mostly be performed in an intuitive rather qualitative way, as - at the correct imaging conditions - black contrast can be associated with columns of (heavy) atoms (Cowley & Iijima, 1972). However, the electron beam carries quantitative information of the potential field in the crystal (Cowley, 1975) and it is possible in principle to use an image for evaluation of the finer details of the structure, such as the degree of occupancy at particular atomic sites. We have been facing this problem in connection with studies of crystals having alkali atoms in tunnels, and here we present results obtained on intergrowth tungsten bronzes.

Many crystal structures can be described as a polyhedral framework forming tunnels, in which suitably sized ions can be accommodated. If the framework contains transition-metal ions with an easily variable oxidation state, there are possibilities for a variation in the degree of filling of the tunnel sites, resulting in non-stoichiometry.

The alkali tungsten bronzes are typical representatives of this class of materials. Their general formula is A_xWO_3, where A is an alkali metal (or one of a few other electropositive metals). They have structures consisting of frameworks of corner-sharing WO_6 octahedra of WO_3 stoichiometry. Four-, five- or six-membered rings of octahedra form tunnels in which the A atoms can be accommodated. Several types of tungsten bronzes exist. The one we are concerned with here is the intergrowth tungsten bronze, ITB (Hussain & Kihlborg, 1976), which forms with K, Rb, and Cs for x values below 0·10 (Hussain, 1978*a*). The structure of ITB can be considered as lamellar intergrowth of hexagonal tungsten bronze, HTB (Magnéli, 1953), containing wide six-membered rings which form hexagonal tunnels, and a slightly distorted 'square' network of WO_3 type, as shown in Fig. 1.

The width of the intergrowing slabs may vary, in which case different ordered members of a structural family can form. The ratio of the number of tunnels, *i.e.* alkali sites, to the number of tungsten atoms will generally differ among these members, thereby allowing a variable stoichiometry x. However, the alkali content will also vary if the occupancy of the tunnel sites is not restricted to a fixed value. The stoichiometry is thus a bivariant problem. Since the high-temperature preparation procedure so far applied almost invariably yields polyphasic samples, which are mixtures of several different members, the phase composition has to be estimated from a statistical analysis of a number of electron diffraction (ED) patterns or HREM images recorded from crystal fragments in the sample (Hussain, 1978*b*).

If the gross composition of the sample is known, the average tunnel occupancy can be calculated. This type of analysis has been made recently on Cs ITB samples (Kihlborg, Fernandez, Laligant & Sundberg, 1988). Although the statistical significance is limited, it was found that the tunnel occupancy seems to vary widely; from about 35% to near 90%. The correlation with sample composition was found to be very weak, but a marked increase in the occupancy with increasing preparation temperature was observed. Chemical energy-dispersive spectroscopy (EDS) microanalysis of individual fragments, structurally characterized by ED, has been made on the related fully oxidized 'bronzoids', $Cs_xNb_xW_{1-x}O_3$ (Sharma, 1985), but has not yet been applied to the pure bronzes owing to lack of suitable equipment.

The use of X-ray diffraction methods is seriously hampered by the difficulties of obtaining true single-phase samples, by the complexity of the powder patterns, and by the inherent disposition towards defects and disorder in single crystals. One structure determination has, however, been made of an ITB phase; a caesium (1,7)-ITB crystal found after 35 crystals had to be rejected because they gave poor X-ray diffraction patterns. The structure refinement indicated that the tunnels were only partially filled with caesium; the occupancy was found to be 62% (Hussain, 1977).

A more direct way to determine the tunnel occupancy on a very local level would be to measure the contrast at the corresponding places in HREM images. The present investigation was initiated as an attempt in this direction. It was also impelled by the frequent observation that in very high-resolution

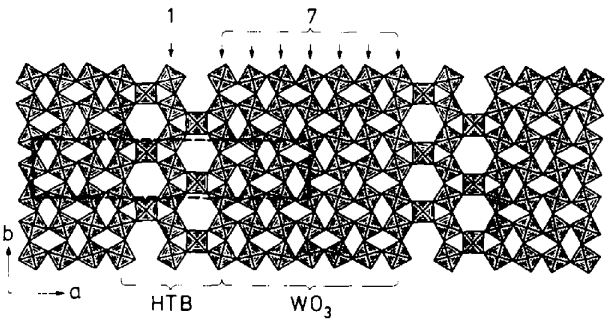

Fig. 1. Structure model of a member of the ITB family, depicted in terms of WO_6 octahedra sharing corners in three dimensions. The alkali atoms (not indicated) are located in the six-sided tunnels in the HTB-type slabs. One unit cell is marked by dashed lines. Since there are one and seven rows of octahedra between the centers of the tunnels in one repeat unit, this particular structure is designated (1,7)-ITB.

images of thin Cs ITB crystals the contrast at the center of the tunnels is nearly equal to that of the tungsten atoms, making the tunnels almost impossible to recognize.

Rieck, Langley & Eyring (1982) have made a HREM investigation of HTB-type potassium vanadium fluoride in which they tried to estimate the degree of filling of the tunnels by comparing calculated and observed images. The latter were averaged by Fourier filtering. They came to the conclusion that only very rough estimates were possible owing to the uncertainties in the imaging parameters.

Experimental

The ITB specimens investigated were from two samples of gross compositions $Rb_{0\cdot10}WO_3$ and $Cs_{0\cdot09}WO_3$. The latter sample is essentially monophasic, containing only (1,4)-ITB, and should therefore have a tunnel occupancy of 54%. These samples had been prepared by heat treatment of appropriate mixtures of rubidium or caesium tungstate, tungsten trioxide and tungsten dioxide, as described previously (Hussain, 1978*a*; Kihlborg, Fernandez, Laligant & Sundberg, 1988). Part of the sample was ground in an agate mortar, dispersed in *n*-butanol and collected on a holey carbon film on a standard copper grid.

The specimens were examined in a JEOL JEM-200CX electron microscope equipped with a THG2 top-entry goniometer stage and LaB_6 cathode, operated at 200 kV. Attached to the microscope is a Gatan 622 TV system including a YAG single-crystal screen and an image intensifier. The HREM images were mostly recorded with a Grundig BK-300 one-inch video recorder. The crystal fragments were aligned with the beam parallel to the *c* axis, allowing the projection along the tunnels to be imaged (*cf.* Fig. 1).

Suitable images or image series were subsequently grabbed from the tape with the use of a Kontron IPS image processing system. A gliding average real-time-video function was thereby used, defined by the formula

$$A_n = [C/(C+1)]A_{n-1} + [1/(C+1)]I_n$$

where I_n is the nth incoming TV frame, A is the time-averaged image and C is a constant. With $C = 3$ as a suitable time constant, 90% of the image intensity comes from the last eight frames (0·32 s). Since specimen drift is one of the more serious problems in HREM, the advantage of such a short integration time is obvious. The images were digitized to 768×512 or 512×512 pixels size and 2^8 grey levels. In some cases the image processing system was used on-line with the microscope and images directly transferred to its 4 Mbyte image memory. Linear histogram normalization, but no further contrast manipulation, was applied to the stored images and densitometric (intensity) measurements made on selected parts.

Simulated images were calculated on a VAX 11/750 computer using a locally modified version of the multislice program suite *SHRLI*-81 (O'Keefe, 1984) in a 128×128 matrix version. The calculated images were transferred to the IPS system for densitometric measurements and comparison with the observed ones. The structure model used in these calculations was that obtained by Hussain (1977) for the (1,7) Cs phase based on X-ray diffraction data. The (1,4)-ITB coordinates were derived from the (1,7) model by elimination of three octahedral rows in each WO_3-type slab. The dimensions of the primitive unit cell used for the (1,4) model were $a = 24\cdot051$, $b = 7\cdot344$, $c = 3\cdot918$ Å, $\gamma = 98\cdot78°$, transformed from the *C*-centered orthorhombic cell given by Kihlborg, Fernandez, Laligant & Sundberg (1988).

The following general imaging parameters were used: spherical aberration constant $C_s = 1\cdot2$ mm, focus spread 50 Å, beam divergence 0·5 mrad, objective aperture radius corresponding to 0·42 $Å^{-1}$. Beams out to approximately 1·8 $Å^{-1}$ were included in the phase grating calculations and to 1·15 $Å^{-1}$ or more in the multislice. Slice thickness was 3·9 Å, corresponding to one layer of metal atoms perpendicular to **c**.

Results

A typical image of a rather thick Cs ITB crystal is seen in Fig. 2. The tunnels are quite distinct, as they generally are for thicker crystals. Image calculations for 16–20 slices (60–80 Å) and −1050 Å defocus give reasonable agreement with this image (see inset).

For quantitative evaluation of the contrast the thick regions are of no use, however, as the observed resolution is poor and the detailed appearance of the image depends to a great deal on thickness, slight crystal tilt and other parameters that are difficult to control

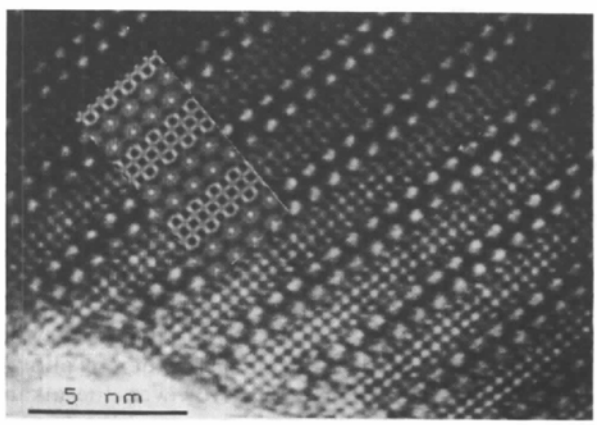

Fig. 2. Image of a thick fragment of Cs (1,4)-ITB. Simulated image inserted (thickness 78 Å, defocus −1050 Å).

or measure. One should therefore look at the thinner parts, where images such as those of Fig. 3 are seen.

Fig. 3(*a*) is recorded close to Scherzer focus and shows clearly the hexagonally arranged dots corresponding to the tungsten and caesium atoms in the HTB-type slabs. The structure model is shown in Fig. 4 (to be compared with Fig. 1). As seen, there are three rows of metal atoms of interest, marked *A*, *B* and *C*. *A* and *C* are equivalent and contain alternate alkali-metal and tungsten atoms, while row *B* contains only tungsten. Simulated image calculations show that a difference in intensity of the alkali and tungsten dots along *A* and *C* should practically always be observed for Rb and in most cases also for Cs.

Two focus series of simulated images are depicted in Fig. 5; one based on Cs (1,4)-ITB with 62% Cs in the tunnels, which is slightly more than should be present (see above), and the other on Rb (1,7)-ITB with the same tunnel occupancy. In both these cases the tunnels are clearly seen, at least for some defocus values. This is obvious in Fig. 6, where the calculated intensity at the Cs and W positions in rows of types *A* and *C* is plotted *versus* defocus for the Cs case. A curve corresponding to the total image contrast is also shown. Intensity minima for both atoms (atoms black), with a simultaneous contrast maximum, occur for defocus values near −450 Å (close to Scherzer focus) and −1250 Å. At both these focus settings the difference in intensity between Cs and W is not very large. At the focus settings giving reversed contrast (atoms white), however, around −100 and −800 Å, one can see that there should be a marked difference. The reverse contrast differences become larger for thicker crystals, while for crystals thinner than six slices the differences near Scherzer focus are more pronounced. Even for 100% Cs occupancy there should be significant variation along these rows, especially at reversed contrast, as calculations indicate.

It is a matter of fact that one only very rarely sees the expected contrast variation along the tunnel rows in Cs ITB crystals. Some typical images are shown in Fig. 3: a near-Scherzer-focus image in (*a*) and three images with reversed contrast in (*b*)-(*d*). The latter are taken at a defocus of approximately −900 Å and they differ from each other by approximately 50–60 Å. In none of these images can a distinct alternation in

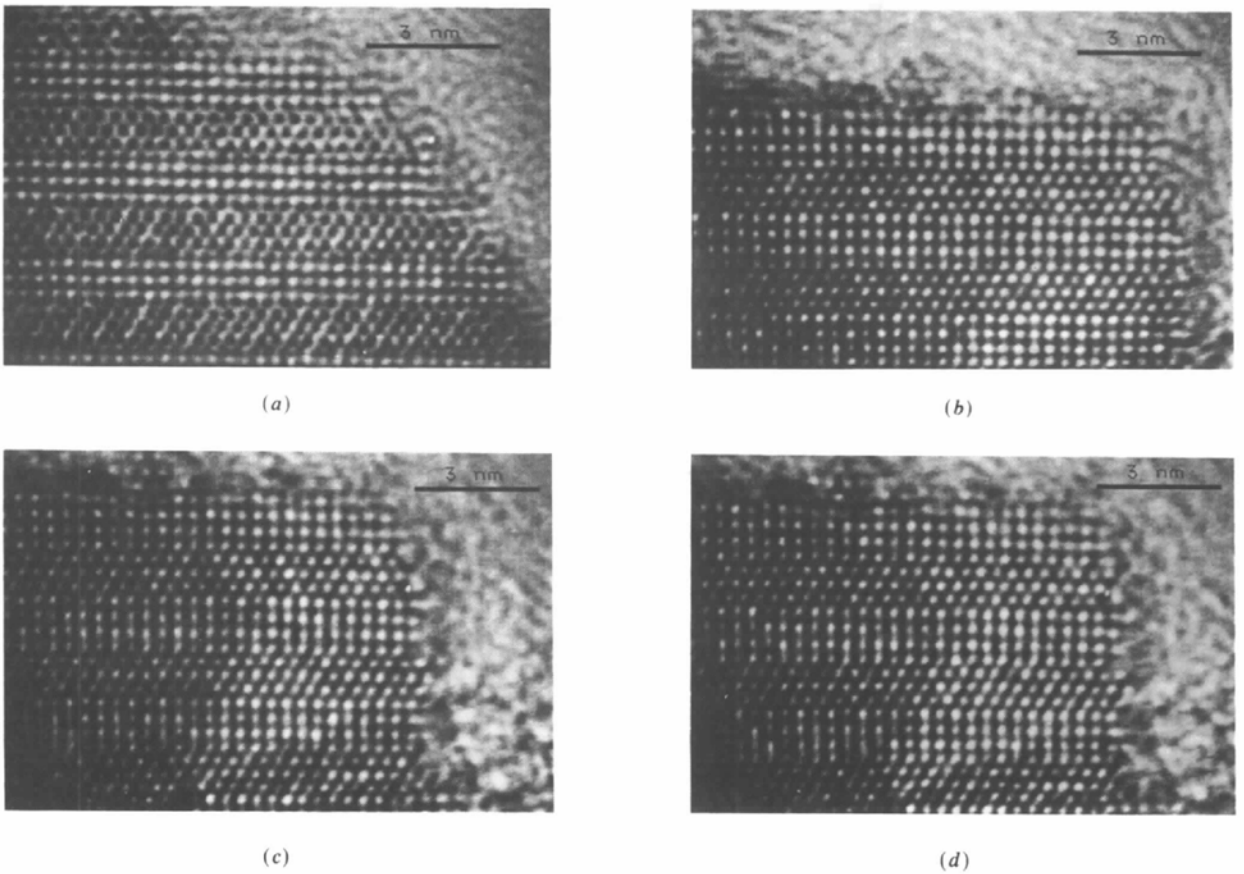

(*a*) (*b*) (*c*) (*d*)

Fig. 3. A thin edge of a Cs (1,4)-ITB crystal imaged (*a*) at a defocus of approximately −500 Å, and (*b*)-(*d*) with reversed contrast at around −900 Å. (*b*)-(*d*) are recorded in sequence with focus steps of approximately 60 Å.

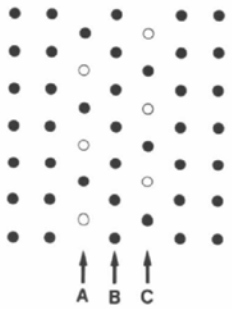

Fig. 4. Metal-atom arrangement in the HTB part of a $(1,n)$-type ITB (*i.e.* containing double tunnel rows). Tungsten atoms: filled circles; alkali atoms: open circles. The outer atom rows belong to WO_3 slabs (*cf.* Fig. 1). The orientation is the same as in Fig. 1 but turned through 90° compared with Figs. 3 and 5.

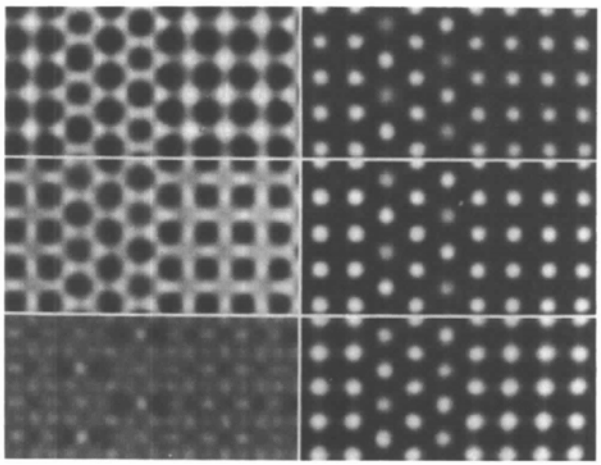

(*a*)

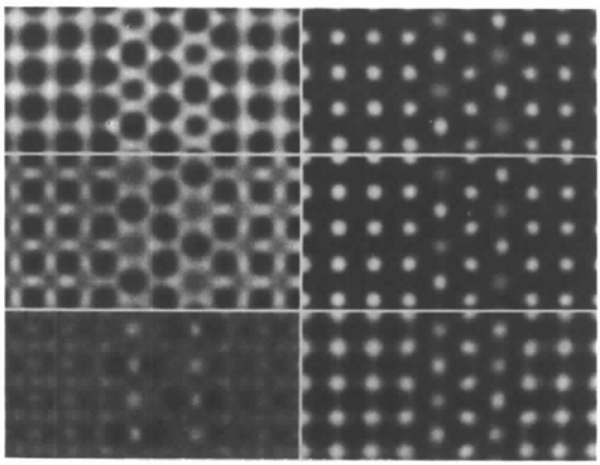

(*b*)

Fig. 5. Simulated images of (*a*) Cs (1,4)-ITB and (*b*) Rb (1,7)-ITB. Tunnel occupancy: 0·6, thickness: 23 Å (six slices), defocus: −450 (top left) to −950 Å (bottom right) in steps of 100 Å.

tunnel rows be observed. The weak double periodicity that can be seen in some parts along the HTB slabs extends across the slab and is as pronounced in the middle, at the *B* row. Thus it is a very vague indication of the tunnel positions. It is a rather general observation that when a modulation is seen in thin crystals, it is present also in the *B* rows, contrary to what one should expect.

On rare occasions one can find regions in very thin parts where a clear modulation along the *A* and *C* rows is visible. One example is shown in Fig. 7(*a*). This is a thin edge of a rather thick crystal that has been subjected to the beam for quite some time. The patchy character has developed during the irradiation and indicates that the crystal is slowly deteriorating in the beam. Densitometric traces down the rows *A*, *B* and *C* in the rightmost HTB slab are presented in Fig. 7(*b*). Here we can see the expected variation in *A* and *C*, with W atoms (deep minima) in *A* at the same level as Cs atoms (small minima) in *C*, and *vice versa*, and no obvious double periodicity in *B* except very locally. One can observe the same modulation also in other HTB slabs of this image, but there are also regions where it is practically absent.

Two images of a rubidium (1,11)-ITB crystal are shown in Fig. 8, one at correct (*a*) and the other at inverse contrast (*b*). The tunnels can be discerned in (*a*) but are not clearly revealed in (*b*). Densitometric traces along the same *A*-type row (arrowed) in the two images are shown in Fig. 8(*c*). In the row of Fig. 8(*a*) the observed Rb/W contrast ratio is approximately 0·75 as an average, while the ratio expected from simulations is close to 0·5 at −500 Å defocus, where the best agreement with the appearance of the WO_3-type part is found. However, the calculated ratio increases to 0·7 at −450 Å defocus, so the difference is hardly significant. As for Cs ITB, there is also in this case a cross over in the intensity of Rb compared with W around −950 Å defocus (for a thickness of six slices, *cf.* Fig. 6) and Fig. 8(*b*) might have been

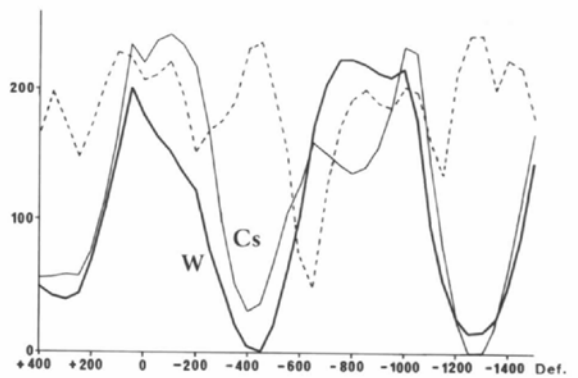

Fig. 6. Intensity at W and Cs positions along the tunnel rows (*A* and *C* in Fig. 4) *versus* defocus, calculated for Cs (1,4)-ITB with 62% Cs in the tunnels. Thickness 23 Å (six slices). Dashed curve indicates image contrast.

recorded close to this defocus. However, the appearance of the WO_3-type net, distinct white dots on a dark background, is compatible only with calculated images at a slightly more positive defocus value, where there is a marked difference between the Rb and W positions. Again, there seems to be a discrepancy between the expected and observed contrast at the tunnel positions.

In another region of the same crystal (Fig. 9), recorded near Scherzer focus, the tunnels are clearly seen in part of the HTB-type slab. The contrast maximum in the tunnel is not always at its center, however, but mostly more or less displaced in one and the same direction. If this were due to a slight

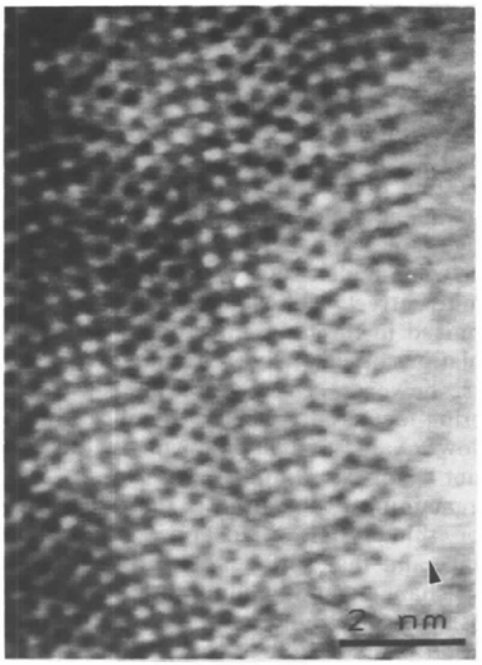

(*a*)

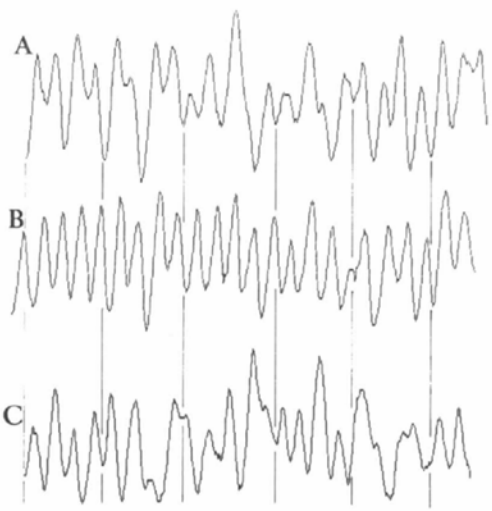

(*b*)

Fig. 7. (*a*) Image of a thin edge of a crystal of Cs (1,4)-ITB, subjected to the focused beam for 5–10 min. The patchy character has developed during the observation. (*b*) Densitometric traces along the rightmost HTB rows: *A* = left, *B* = middle, *C* = right (arrowed). The traces are from the top downwards and the vertical lines indicate corresponding positions perpendicular to the row.

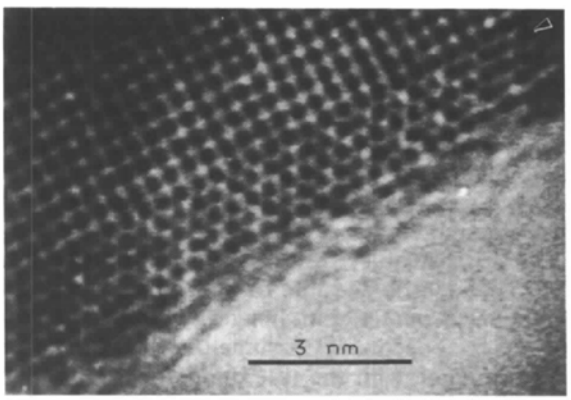

(*a*)

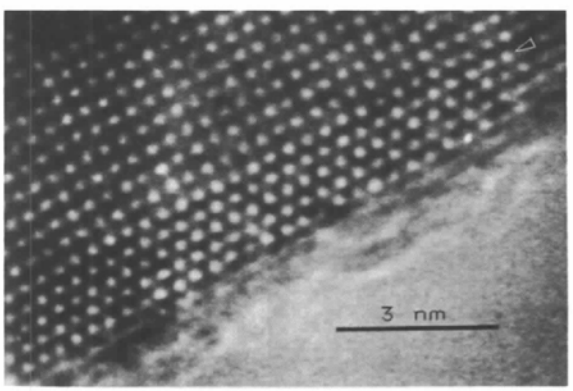

(*b*)

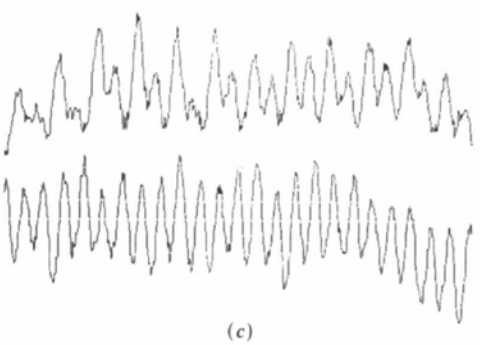

(*c*)

Fig. 8. The edge of an Rb (1,11)-ITB crystal recorded (*a*) near Scherzer focus, −450 to −500 Å, and (*b*) with reversed contrast at approximately −900 Å defocus. (*c*) Densitometric traces along the rows marked in (*a*) (top) and (*b*) (bottom), starting at the arrows.

beam tilt, one should expect the same effect over the whole image. Crystal tilt, on the other hand, should give an effect that increases with thickness, but the reverse is true (note the almost centered spot in the leftmost tunnels). It therefore seems likely that this is not an imaging artefact but a real effect of structural origin.

Discussion

It has been shown above that the observed HREM images of thin crystal fragments of Cs and Rb ITB frequently differ from those expected from image simulations. The HTB tunnels are mostly rather poorly revealed because the contrast in the center is as pronounced as that due to the surrounding tungsten atoms. A number of alternative explanations for this can be imagined.

The primary objective of the present investigation was to see if it is possible to assess the bulk tunnel occupancy from HREM images. The first guess is thus that the occupancy assumed in the calculations does not agree with the true one. However, at least in the Cs case the deviation cannot be large, as the specimen is from a practically monophasic sample and the amount of Cs available is given from the preparation. Moreover, even full occupancy of the tunnels should not make them 'disappear' for all defocus values.

Beam and crystal tilt are experimental parameters which are difficult to keep under close control, but they cause severe distortions in the image symmetry before they give any noticeable change of contrast in the tunnels.

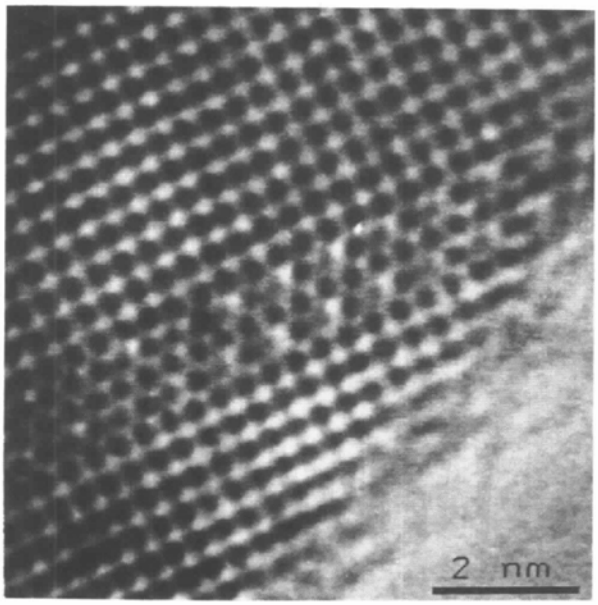

Fig. 9. Image of a different part of the same crystal as in Fig. 8. Here the tunnels are clearly revealed in most of the HTB slab, except in the leftmost part. The contrast in the tunnels varies but the maximum is often displaced to the side, while in others it is well centered and has stronger contrast.

The image simulation procedure is only an approximation, but since we are dealing with very thin crystals, the method should be sufficiently accurate (Cowley & Moodie, 1959; Goodman & Moodie, 1974). Small changes from the assumed values of the imaging parameters (focus spread, beam divergence and spherical aberration) are also not likely to affect the simulated images in the required way. Only thicknesses below ten slices (40 Å) gave general agreement between calculated and observed thin-edge images. Within this range different thicknesses give rather similar images but with a focus shift towards less negative values with increasing thickness. Most calculations were made assuming neutral atoms, which is not quite correct, as it is known that the alkali atoms are ionized in the tungsten bronzes, at least partly. Calculations based on ionized atoms give very similar results, however. This is not unexpected, as the scattering-factor curves differ significantly only for very low θ values, much below the region where the relevant beams are found.

A remaining explanation is that the structure of the very thin crystals differs appreciably from that of the bulk and that surface effects play a significant role. A change could be induced by the beam in the microscope, but could also be caused by surface oxidation or hydration of the specimen before it is introduced into the column.

Jefferson, Uppal, Smith, Gopalakrishnan, Ramanan & Rao (1984) and Smith, Bursill & Jefferson (1986) have studied bismuth tungsten bronze using 400 or 500 kV microscopes. This phase has a single-row (n)-ITB structure and in the thin parts the tunnels generally show up with low contrast in the center, indicating a low degree of filling. The latter authors note that electron irradiation leads to a depletion of Bi atoms from the tunnels and associate this with a build up of atom layers at the edge of the crystal. They also observe 'metallization' of the WO_3 part nearest to the edge, which they suggest is caused by preferential electron-stimulated desorption of oxygen. In images published recently by Dobson, Hutchison, Tilley & Watts (1987) of barium ITB bronze, the tunnels are clearly revealed in the thinnest parts of the crystal. Also, this structure has HTB slabs only one tunnel row wide, and the tunnels are obviously filled to a varying degree with barium; some appear empty or nearly so. These authors do not report any change of the crystals in the beam, however.

In the present study we have not observed any marked changes in the appearance of the tunnels during beam irradiation and preferential loss of alkali does not seem to occur. However, samples subjected to the focused beam for a long time get a patchy

appearance (*cf.* Fig. 7*a*), obviously due to evaporation of larger areas of the crystal, and in such instances the tunnels might become clearly visible, as exemplified above. Both Cs and Rb seem to be rather tightly bonded in the tunnels owing to their large size.

We believe that the non-appearance of the tunnels in the very thin regions of Cs and Rb ITB crystals is due to an appreciable surface reconstruction, in which the partly occupied tunnels may act as traps for tungsten atoms. These could come from any part of the crystal surface but it seems likely that they originate in the octahedra immediately surrounding the tunnels. Some support for this is found in the variation in contrast that is often seen also along the *B* rows in the HTB slabs. It is even possible that the whole octahedral framework is concertedly shifted by $\frac{1}{2}\mathbf{b}$ in the surface layers, whereby the tunnels become closed at the ends. The contrast at the Cs and W positions along the *A* and *C* rows would become more similar by that mechanism, as observed. This shifted surface structure would be similar to the crystal structure of $WO_3{\cdot}\frac{1}{3}H_2O$, determined by Gerand, Nowogrocki & Figlarz (1981). Hydroxyl groups are indeed likely to be present on the surface of the bronze, saturating the dangling bonds created when the crystal is crushed.

In thin parts of crystals that are deteriorating by prolonged heating in the beam, the tunnels do indeed show up with a contrast compatible with a low and variable alkali content (Fig. 7*a*). It seems reasonable to believe that in these cases, when evaporation obviously takes place, most misplaced or trapped surface atoms have been removed. The off-center displacement frequently seen when the contrast of the spot in the tunnel is weak, exemplified here in the rubidium case (Fig. 9), may be due to one or two tungsten atoms in the surface layer. A location of such atoms at the center of the tunnel would give a very unsatisfactory coordination.

Finally, one has to remember that a carbonaceous contamination layer usually builds up on the surfaces of the specimen in the microscope, as visible for example at the edge of Fig. 3. It is hard to see, however, that such a layer could give rise to contrast changes preferentially at the tunnel positions. One cannot exclude, however, that it might contribute to inducing surface rearrangements.

It seems of little use to speculate further about the possible surface structures that could explain the effect observed here. A structural study of the surface by other methods seems necessary in order to reveal its true nature.

References

COWLEY, J. M. (1975). *Diffraction Physics*. Amsterdam: North-Holland.

COWLEY, J. M. & IIJIMA, S. (1972). *Z. Naturforsch. Teil A*, **27**, 445-451.

COWLEY, J. M. & MOODIE, A. F. (1959). *Acta Cryst.* **12**, 360-367.

DOBSON, M. M., HUTCHISON, J. L., TILLEY, R. J. D. & WATTS, K. A. (1987). *J. Solid State Chem.* **71**, 47-60.

GERAND, B., NOWOGROCKI, G. & FIGLARZ, M. (1981). *J. Solid State Chem.* **38**, 312-320.

GOODMAN, P. & MOODIE, A. F. (1974). *Acta Cryst.* A**30**, 280-290.

HUSSAIN, A. (1977). *Chem. Scr.* **11**, 224-227.

HUSSAIN, A. (1978*a*). *Acta Chem. Scand. Ser. A*, **32**, 479-484.

HUSSAIN, A. (1978*b*). *Chem. Commun. Univ. Stockholm*, No. 2.

HUSSAIN, A. & KIHLBORG, L. (1976). *Acta Cryst.* A**32**, 551-557.

JEFFERSON, D. A., UPPAL, M. K., SMITH, D. J., GOPALAKRISHNAN, J., RAMANAN, A. & RAO, C. N. R. (1984). *Mater. Res. Bull.* **19**, 535-537.

KIHLBORG, L., FERNANDEZ, M., LALIGANT, Y. & SUNDBERG, M. (1988). *Chem. Scr.* **28**, 71-75.

MAGNÉLI, A. (1953). *Acta Chem. Scand.* **7**, 315-324.

O'KEEFE, M. A. (1984). In *Electron Optical Systems for Microscopy, Microanalysis and Microlithography*, edited by J. J. HREN, F. A. LENZ, E. MUNRO & P. B. SEWER. *Proc. 3rd Pfeffercorn Conf.* SEM Inc., AMF O'Hare, IL 60666, USA.

RIECK, D., LANGLEY, R. & EYRING, L. (1982). *J. Solid State Chem.* **45**, 259-275.

SHARMA, R. (1985). *Acta Chem. Scand. Ser. A*, **39**, 397-403.

SMITH, D. J., BURSILL, L. A. & JEFFERSON, D. A. (1986). *Surf. Sci.* **175**, 673-683.